UC Irvine
UC Irvine Previously Published Works

Title

Theoretical and Experimental Electrophysiology in Human Neocortex: Multiscale Dynamic Correlates of Conscious Experience

Permalink

https://escholarship.org/uc/item/3443243d

ISBN

9783527411986

Authors

Nunez, Paul L
Srinivasan, Ramesh
Ingber, Lester

Publication Date

2013-08-14

DOI

10.1002/9783527671632.ch06

Copyright Information

Peer reviewed

Part Three
Nonlinear Dynamics: the Brain and the Heart

6
Theoretical and Experimental Electrophysiology in Human Neocortex: Multiscale Dynamic Correlates of Conscious Experience

Paul L. Nunez, Ramesh Srinivasan, and Lester Ingber

6.1
Introduction to Brain Complexity

6.1.1
Human Brains and Other Complex Adaptive Systems

In this chapter, human brains are treated as preeminent complex systems with consciousness assumed to emerge from dynamic interactions within and between brain subsystems [1–9]. Given this basic premise, we first look for general brain features underlying such complexity and, by implication, the emergence of consciousness. We then propose general dynamic behaviors to be expected in such systems, and outline several tentative connections between theoretical predictions and experimental observations, particularly the large-scale (cm) extracranial electric field recorded with electroencephalography (EEG).

Emergence generally occurs in hierarchically organized physical and biological systems where each higher level of complexity displays novel emergent features based on the levels below it, their interactions, and their interactions with higher levels. In the field of *synergetics* (the science of cooperation and self-organization in complex systems), the critical importance of top-down and bottom-up interactions across the scales of *nested hierarchical systems* is widely recognized and may be labeled *circular causality* [4].

A second salient feature of many complex systems is the presence of *nonlocal interactions* in which dynamic activity at one location influences distant locations, without affecting intermediate regions as demonstrated in mammalian brains by corticocortical fibers [5,7,8], and in human social systems by modern long distant communications facilitating *small-world* behavior [9,10]. The high density of short-range (local) brain connections coupled with an admixture of long-range (nonlocal) connections favors small world behavior. Small worlds can promote high complexity [5,9,10]; they also appear to be abundant in brain structural networks, across systems, scales, and species [9].

But, what makes brains so special? How do they differ from hearts, livers, and other organs? All organ systems are enormously complicated structures, able to

repair themselves and make detailed responses to external control by chemical or electrical inputs. Yet, only brains yield the amazing phenomenon of consciousness [1–6]. Complex adaptive systems, for which human brains appear to provide prominent examples, are generally composed of smaller parts interacting both within and across spatial scales. They typically exhibit emergent behavior not obviously predictable from knowledge of the individual parts and have the added capacity to learn from experience and change their global behaviors by means of feedback processes. Other examples include stock markets, social systems, ecosystems, and other living systems [9,11,12], any of which can demonstrate both circular causality and nonlocal interactions. Several general features seem to distinguish mammalian brains from other complex biological and physical systems, especially the hallmark of rich hierarchical interactions between multiscale brain substructures, somewhat analogous to top-down and bottom-up interactions in social systems between persons, cities, and nations.

6.1.2
Is "Consciousness" a Four-Letter Word?

Consciousness is often defined as an internal state of awareness of self, thoughts, sensations, and the environment: a circular definition to be sure, but useful as a starting point. Consciousness may be viewed from both inside and outside. Our internal experiences are fundamentally private; only you can be certain that you are actually conscious. External observers may affirm your consciousness based on language, purposeful behavior, attention to the environment, body language, facial expressions, and so forth. External observers can be quite wrong, however. Discrepancies between internal and external views may occur with dreaming subjects, the nonverbal right hemisphere of a split-brain patient, and in coma, or Alzheimer patients in various stages of awareness. In addition, both internal and external observations have, at best, very limited access to the unconscious, which receives information from the external world that is stored in memory and profoundly influences behavior.

The environment for consciousness studies has not always been friendly. Only in the past 20 years or so has the study of consciousness been widely considered to fall within the purview of genuine scientific inquiry. In the past, time spent in such pursuits was typically considered a career-limiting move, perhaps analogous to some views on the ontology of quantum mechanics, known as the "measurement problem." We aim to skirt much of this controversy by clearly distinguishing three separate questions: (1) What are the neural correlates of consciousness? (2) What are the necessary conditions for consciousness to occur? (3) What are the sufficient conditions for consciousness to occur? Brain science has made substantial progress in answering the first question, one can only make plausible conjectures about the second question, and almost nothing is known about the third question [3,5,6,13].

In this chapter, we cite brain experiments carried out at several distinct spatial and temporal scales that provide robust neural correlates of observable aspects of consciousness, thereby directly addressing the first of the three basic questions

listed above. To approach the second question, we suggest two interrelated physio-logic-theoretical approaches, applied at different spatial scales of neural tissue that can account for these disparate data, thereby providing a tentative connection between brain anatomy/physiology and conscious processes. No attempt is made here to answer the third question.

6.1.3
Motivations and Target Audiences for this Chapter

We aim here to reach a broad audience including both physical and biological scientists, thereby providing a large-scale road map to previously published work in several overlapping sub fields of brain science. Given space limitations and varied backgrounds of potential readers, an informal format is employed in which (1) reference citations emphasize review articles and textbooks rather than giving credit to original work; (2) metaphors are generously employed to minimize communication barriers, given that many readers are expected to lack expertise in either mathematical physics or neuroscience; (3) with the exception in Section 6.4, most mathematical and other technical details are limited to references. Such approach to a disparate audience may have its detractors; for example, an early critic of author PLN employed the colorful label "motherhood down talk" to voice his impatience. Here we risk such criticisms to aim for a more widely accessible overview of the subject matter. Our metaphors are meant to supplement rather than replace genuine brain theories, several of which have been widely published.

Neuroscientists are typically skeptical of brain analogs, typically for good reason; however, we are *not* claiming that brains are actually just like stretched strings, social systems, quantum structures, resonant cavities, hot plasmas, disordered solids, spin glasses, chaotic fluids, or any other nonneural system. Rather, we suggest that each of these systems may exhibit behavior similar to brain dynamics observed under restricted experimental conditions, including spatial and temporal scales of observation. The multiple analogs then facilitate complementary models of brain reality.

The theoretical work outlined here emphasizes two distinct but complementary theories: the large-scale global standing wave model for EEG [7,8,14–18] and the intermediate scale statistical mechanics of neocortical interactions (SMNI) developed independently by Ingber [11,12,19,20]. These disparate theories are believed to be mutually complementary and complementary to several similar theories of neocortical dynamics [7,12,15]. They provide a quantitative physiological framework for circular causality and critical nonlocal interactions. However, most of our discussion on brain complexity and cognition is independent of the details of these theories; one should anticipate future modifications as new brain data become available.

6.1.4
Brain Imaging at Multiple Spatial and Temporal Scales

Brain imaging may reveal either structure or function. *Computed tomography* (CT) or *magnetic resonance imaging* (MRI) reveal structural changes on monthly or yearly

time scale. By contrast, intermediate time scale methods such as *functional magnetic resonance imaging* (fMRI) and *positron emission tomography* (PET) track functional brain changes over seconds or minutes. Still more rapid dynamic measures are *electroencephalography* and *magnetoencephalography* (MEG), which operate on milli-second time scales, providing dynamic images faster than the speed of thought. The price paid for the excellent temporal resolutions of EEG and MEG is coarse spatial resolution [8,17]. These regional (centimeter scale) data provide many important neural correlates of observable aspects of consciousness, including attention, work-ing memory, perception of external stimuli, mental tasks, and depth of sleep, anesthesia, or coma. Of particular interest are various measures of functional (dynamic) connections between brain regions such as covariance in the time domain and coherence in the frequency domain [2,5,7–9,16,21,22].

Cognitive scientists and clinicians readily accept the low spatial resolution obtained from scalp EEG data, although explorations of EEG methods to provide somewhat higher spatial resolution continue [8,17]. A reasonable goal is to record averages over "only" 10 million neurons at the 1-cm scale in order to extract more details of the spatial patterns correlated with cognition and behavior. This resolution is close to the theoretical limit of spatial resolution caused by the physical separation of sensor and brain current sources. Scalp data are largely independent of electrode size because scalp potentials are severely space-averaged by volume conduction between brain and scalp. Intracranial recordings provide smaller scale measures, with the scale dependent on the electrode size. A mixture of coherent and incoherent sources generates the small- and intermediate-scale intracranial data. Scalp data are due mostly to sources coherent at the scale of at least several centimeters with special geometries that encourage the superposition of potentials generated by many local sources.

Many studies of the brain dynamics of consciousness have focused on EEG, the electric potentials or "brain waves" recorded from human scalps. EEG allows for accurate identification of distinct sleep stages, depth of anesthesia, seizures and other neurological disorders. It also reveals robust correlations of brain activity with a broad range of cognitive processes including mental calculations, working memory, and selective attention. Thus, EEG provides very large-scale and robust measures of neocortical dynamic function. A single electrode yields estimates of synaptic action averaged over tissue masses containing a few hundred million or so neurons. The space averaging of brain potentials resulting from extracranial recording is forced by current spreading in the head volume conductor. Much more detailed local information is obtained from intracranial recordings in animals and epileptic patients. However, intracranial electrodes implanted in living brains provide only very sparse spatial coverage, thereby failing to record the "big picture" of brain function. Furthermore, the dynamic behavior of intracranial recordings depends fundamentally on measurement scale, determined mostly by electrode size. Different electrode sizes and locations can result in substantial differences in recorded dynamic behavior, including frequency content and coherence. Brain structure and its associated dynamic behavior exhibit a multiscale intricate character that reminds us of fractals, suggesting various statistical studies on self-similarity

and scale-free behavior [9]. Thus, in practice, intracranial data provide different information, not more information, than that is obtained from the scalp [8,17].

6.1.5
Multiple Scales of Brain Dynamics in Consciousness

Human consciousness is widely believed to be an emergent property of brain activity at multiple spatial and temporal scales. As an example, we review data obtained using *binocular rivalry*, one of the fundamental paradigms employed to investigate neural correlates of consciousness [21,23–26]. In binocular rivalry, two incongruent images are presented one to each eye; the observer perceives only one image at a time. Thus, while the physical stimuli remain constant, the observer experiences spontaneous alternation in perception between the two competing images. This phenomenon provides a useful window into the neural dynamics underlying conscious experience; the neural inputs from both visual stimuli enter the brain, but the two images can reach the level of conscious awareness only one at a time.

Experimental studies of binocular rivalry have been carried out in monkeys and humans in order to investigate neural correlates of conscious perception at the single-neuron, local field potential (intracortical-millimeter), and EEG or MEG (centimeter) scales. The dynamics observed depend on the spatial and temporal scale of the recording. In monkeys, measuring the firing rate (number of action potentials/second) of cells in different structures within the visual cortex (in the occipital lobe) has shown that the activity of most cells in primary visual cortex (where the inputs arrive from eyes via the thalamus) is not modulated by conscious perception [23,24]. Further up the visual hierarchy, cells tuned to the features of the rivaling stimuli modulate their firing rate with the changing conscious perception. This might seem to suggest that activity at local scales at the top of the visual hierarchy determines the conscious experience. However, other studies using local field potentials, measuring average synaptic activity in localized cortical populations in primary visual cortex, have shown that low-frequency (<30 Hz) power and coherence in primary visual areas are enhanced when the stimulus is perceived [26], even though the firing rate of the cells is not significantly modulated.

The Gail *et al.* [26] study suggests that increased synchronization of synaptic activity in early visual areas is correlated with conscious percept. Finally, studies in human subjects using steady state visual evoked potentials [21,22] have demonstrated large-scale network activity modulated by conscious perception. In these later studies, incongruent flickering stimuli are presented, one to each eye while conscious perception alternates between the images presented to each eye. In contrast to the changes in magnitude of activities observed at local scales in the monkey studies, the main finding of the human studies is a more integrated scalp coherence pattern in each frequency band, observed with conscious perception of the stimulus flickering at the matching frequency. Thus, conscious perception, in these experiments, occurs with enhanced dynamic "binding" of the brain hemispheres within the theta (4–7 Hz) or alpha (8–13 Hz) frequency bands. If we

extrapolate from the monkey data to humans, the implication is that different types of dynamics occur at different spatial scales (and frequency bands) underlying conscious perception. In addition, dynamic processes occurring in other frequency bands can remain "unbound," allowing other brain networks (unrelated to the stimulus) to engage in independent actions.

6.2
Brief Overview of Neocortical Anatomy and Physiology

6.2.1
The Human Brain at Large Scales

In this section, we outline some of the basic anatomy and physiology that must underpin brain dynamic behavior, thereby providing background material for Sections 6.3–6.5. The three main parts of the human brain are *brainstem*, *cerebellum*, and *cerebrum* as indicated in Figure 6.1a. The brainstem, which sits at the top of the spinal
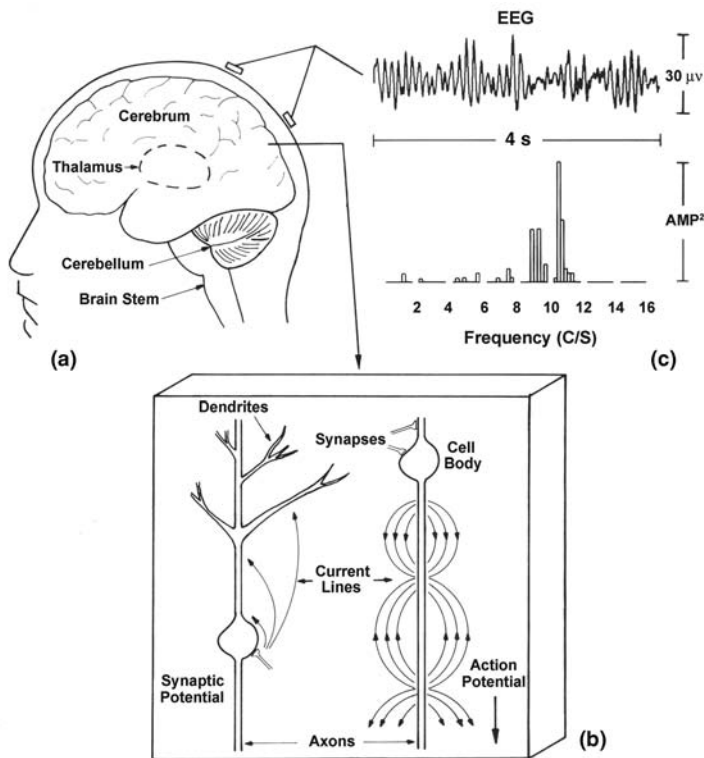

Figure 6.1 (a) Main parts of human brain: *brainstem*, *cerebellum*, and *cerebrum*. (b) Synaptic and action potential current sources. (c) Sample EEG record and spectrum [5,7,8].

cord, relays signals (*action potentials*) along nerve fibers in both directions between spinal cord and higher brain centers. The cerebrum is divided into two halves or *cerebral hemispheres*. The outer layer of the cerebrum is the *cerebral cortex*, a folded, wrinkled structure with the average thickness of 3–4 mm and containing roughly 10^{10} *neurons*. Neurons are nerve cells with many branches similar to a tree or bush. Long branches called *axons* carry electrical signals away from the cell to other neurons. The ends of axons consist of *synapses* that send chemical *neurotransmitters* to the tree-like branches (*dendrites*) or cell body (*soma*) of target neurons as indicated in Figure 6.1b. The surface of a large cortical neuron may be covered with 10 000 or more synapses transmitting electrical and chemical signals from other neurons. Much of our conscious experience involves the interaction of cortical neurons, but this dynamic process of neural network (*cell assembly*) behavior is poorly understood. The cerebral cortex also generates most of the electric (EEG) and magnetic (MEG) fields recorded at the scalp. Many drugs including caffeine, nicotine, and alcohol alter brain function; drugs work by interacting with specific chemical (*neurotransmitter*) systems.

Figure 6.1c depicts 4 s of an electroencephalographic record, the electric potentials recorded from a person with electrodes held against his scalp by elastic caps or bands. Also shown is the corresponding frequency spectrum; in this case oscillations are near 10 Hz, the usual alpha state of waking relaxation with closed eyes. Some of the current generated by neurons in the cerebral cortex crosses the skull into the scalp and produces scalp currents and electric potentials typically in the 10–200 μV range.

6.2.2
Chemical Control of Brain and Behavior

Neurons and cell assemblies communicate both electrically and chemically. *Action potentials* are transmembrane waveforms that travel along axons to synaptic endings that release chemical neurotransmitters to produce specific responses in each target cell (*postsynaptic neuron*); the type of response is determined by the particular neurotransmitter. Each neurotransmitter exerts its postsynaptic influence by binding to specific *receptors*, chemical structures in cell membranes that bind only to matching chemicals. Drugs also work by binding to specific receptors.

The *neuromodulators* are a class of neurotransmitters that regulate widely dispersed populations of neurons. Like hormones, they are chemical messengers, but neuromodulators act only on the central nervous system. In contrast to synaptic transmission of neurotransmitters, in which a presynaptic neuron directly influences only its target neuron, neuromodulators are secreted by small groups of neurons, and diffuse through large areas of the nervous system, producing global effects on multiple neurons. Unlike other neurotransmitters, neuromodulators spend substantial time in the cerebrospinal fluid (CSF) influencing the overall activity of the brain; in physical science parlance, they act as the brain's *control parameters*. As such they are implicated in switching brain dynamics between the extremes of full global coherence (all parts of the brain acting together) and full

isolation (each part doing its own thing) [5,27]. It has also been suggested that brain dynamic complexity and, by implication, healthy consciousness is largest at intermediate states between these extremes [2,9].

6.2.3
Electrical Transmission

While chemical control mechanisms are relatively slow and long lasting, electrical events turn on and off much more quickly. Electrical transmission over long distances is by means of action potentials that travel along axons at speeds up to 100 m/s in the peripheral nervous system, typically 6–9 m/s in the corticocortical axons (white matter), and much slower (cm/s) within cortical tissue (gray matter). The remarkable physiological process of action potential propagation is analogous to electromagnetic wave propagation along transmission lines, although its physical basis, rooted in selective nonlinear membrane behavior, is quite different.

Synaptic inputs to a target neuron are of two types: those that produce *excitatory postsynaptic potentials* (EPSPs) across the membrane of the target neuron, thereby making it easier for the target neuron to fire its own action potential and the *inhibitory postsynaptic potentials* (IPSPs), which acts in the opposite manner on the target neuron. EPSPs produce local membrane *current sinks* with corresponding distributed passive sources to preserve current conservation. IPSPs produce local membrane *current sources* with more distant distributed passive sinks as depicted by the current lines in Figure 6.1c. IPSPs cause positively charged potassium ions to pass from inside to outside the target cell just below the input synapse (active source current). The ions reenter the cell at some distant location (passive sink current). EPSPs cause negatively charged chlorine ions to contribute to local active sinks and distant passive sources. Action potentials also produce source and sink regions along axons as shown in Figure 6.1c; several other interaction mechanisms between adjacent cells are also known.

6.2.4
Neocortex

Cerebral cortex consists of *neocortex*, the outer layer of mammalian brains plus smaller, deeper structures that form part of the *limbic system* associated with emotional responses. The prefix "neo" indicates "new" in the evolutionary sense; neocortex is relatively larger and more important in animals that evolved later. Neocortex contains about 80% excitatory and 20% inhibitory neurons [7,28]. Pyramidal cells tend to occupy narrow cylindrical volumes as opposed to the more spherical basket cells. Each pyramidal cell generally sends an axon to the underlying white matter layer; the axon connects to other parts of cortex or to deeper structures. Neocortex surrounds the inner layer of white matter, consisting mostly of *myelinated axons*. Myelin consists of special cells that wrap around axons and increase the propagation speed of action potentials, typically by factors of 5–10.

Cortex exhibits a layered structure labeled I through VI (outside to inside) defined by a basic cell structure common to all mammals.

Figure 6.2 depicts a large pyramidal cell within a *macrocolumn* of cortical tissue, a scale defined by the spatial extent of axon branches (E) that remain within the cortex and send excitatory input to nearby neurons [7,15]. Each pyramidal cell also sends an axon (G) into the white matter layer. In humans more than 95% of these axons are corticocortical fibers targeting the same (*ipsilateral*) cortical hemisphere. The remaining few percent are *thalamocortical fibers* connecting to the thalamus (on either side of the brainstem) or callosal fibers targeting the opposite (*contralateral*) cortical hemisphere. A probe (A) used to record small-scale potentials through the cortical depth is also shown in Figure 6.2. The dendrites (C) provide the surfaces for synaptic input from other neurons, and *J* represents the diffuse current density across the cortex resulting from the membrane current sources and sinks as represented by the expanded picture (F). The macrocolumn shown in Figure 6.2 actually contains about a million tightly packed neurons and ten billion or so synapses; if only 0.1% of neurons were shown, this picture would be solid black.
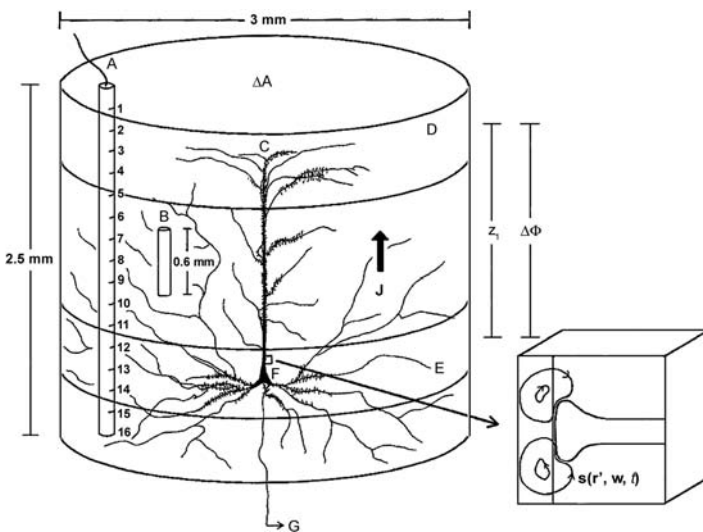

Figure 6.2 The macrocolumn is defined by the spatial extent of axon branches E that remain within the cortex (*recurrent collaterals*). The large pyramidal cell C is one of 10^5–10^6 neurons in the macrocolumn (the figure would be essentially solid black if only as many as 0.1% were shown). Nearly all pyramidal cells send an axon G into the white matter; most reenter the cortex at some distant location (*corticocortical fibers*). Each large pyramidal cell has 10^4–10^5 synaptic inputs F causing microcurrent sources and sinks $s(\mathbf{r}, \mathbf{w}, t)$. Field measurements can be expected to fluctuate greatly when small electrode contacts A are moved over distances of the order of cell body diameters. Recordings at a somewhat larger scale are represented by the volume B [7].

Table 6.1 Spatial scales of cortical tissue structure related to function.

Structure	Diameter (mm)	# Neurons	Anatomical description
Minicolumn	0.03	10^2	Spatial extent of inhibitory connections
Module	0.3	10^4	Input scale for corticocortical fibers
Macrocolumn	3.0	10^6	Intracortical spread of pyramidal cell
Region	50	10^8	Brodmann area
Lobe	170	10^9	Areas bordered by major cortical folds
Hemisphere	400	10^{10}	$^1/_2$ brain

6.2.5
The Nested Hierarchy of Neocortex: Multiple Scales of Brain Tissue

The 10 billion or so cortical neurons are arranged in columns at various scales defined by anatomical and physiological criteria, as indicated in Table 6.1. The *cortical minicolumn* is defined by the spatial extent of intracortical inhibitory connections. Minicolumns extend through the cortical depth so their heights are about 100 times their diameters. Each minicolumn contains about 100 pyramidal cells. Inhibitory connections typically originate with the smaller and more spherical basket cells. Inhibitory action tends to occur more in the middle (in depth) cortical layers II, III, and IV.

The *cortical module* is defined by the spatial spread of (excitatory) subcortical input fibers (mostly corticocortical axons) that enter the cortex from the white matter below. This extracortical input from other, often remote, cortical regions is excitatory and tends to spread more in the upper and lower cortical layers (I and VI).

The *cortical macrocolumn* is defined by the intracortical spread of individual pyramidal cells. As indicated in Figure 6.2, a single pyramidal cell sends axons from the cell body that spread out within the local cortex over a typical diameter of 3 mm. Each macrocolumn contains about a million neurons and perhaps a kilometer or so of axon branches. In addition to the intracortical axons, each pyramidal cell sends one axon into the white matter; in humans, most of these reenter the cortex at some distant location.

Inhibitory interactions seem to occur more in the middle cortical layers, and excitatory interactions are more common in the upper and lower layers. Healthy brains seem to operate between the extremes of global coherence and functional isolation. Different neuromodulators tend to operate selectively on the different kinds of neurons at different cortical depths. Neuromodulators can apparently act to control the large-scale dynamics of cortex by shifting it between the extremes of global coherence and full functional segregation, an idea with important implications for several brain diseases including schizophrenia [5,27].

An overview of cortical structure (*morphology*) reveals neurons within minicolumns, modules, macrocolumns, Brodmann regions, lobes, hemispheres, a nested hierarchy of tissue [1,3,6,28]. A plausible picture suggests that each structure interacts with other structures at the same scale as in neuron-to-neuron interactions

Table 6.2 Estimated spatial resolution of recorded potentials or magnetic fields generated by cortical sources.

Recording method	Typical spatial resolution (mm)
Microelectrode of radius ξ	$\geq \xi$
Local field potentials	0.1–1
ECoG (cortical surface)	2–5
Intraskull recording	5–10
Untransformed EEG	50
Untransformed MEG	50
High-resolution EEG	20–30
High-resolution MEG	Unknown

or minicolumn-to-minicolumn interactions. If inhibitory processes within a column are swamped by excitation (too many EPSPs and not enough IPSPs), this overexcited column may spread its excitation to other columns in the positive feedback process *epilepsy*. Cross-scale interactions are also expected. Small cell groups produce chemical neuromodulators that act (bottom up) on neurons in the entire cortex. External sensory stimuli reach small groups of cells in primary sensory cortex that elicit (bottom up) global brain responses, which in turn act top down on smaller scale structures, completing closed loops of circular causality.

The morphology of cerebral cortex, in which complex structures occur at multiple scales, reminds us of *fractals*, which exhibit fine structure at progressively smaller scales [5,9]. Intracranial measurements of electric potential depend strongly on the sizes and locations of recording electrodes, as seen in Figure 6.2. The practice of *electrophysiology*, which consists of recording electric potentials in tissue, spans about five orders of magnitude of spatial scale, as indicated in Table 6.2 [7,8,29]. Measured potentials at any so-called "point" necessarily represent space averages over the volume of the electrode tip, but EEG is exclusively large scale.

6.2.6
Corticocortical Connections Are Nonlocal and "Small World"

The axons that enter the white matter and form connections with other cortical areas in the same hemisphere are the corticocortical fibers, perhaps 97% of all white matter fibers in humans [7,28]. The remaining white matter fibers are either thalamocortical (perhaps 2%), connecting cortex to the deeper thalamus in the "radial" direction, or callosal fibers (perhaps 1%), connecting one cortical hemisphere to the other. In addition to the long (1–15 cm) *nonlocal* corticocortical fibers, neurons are connected by short-range (less than a few millimeters) *local* intracortical fibers as indicated in Figure 6.2. The density of corticocortical fibers relative to thalamocortical fibers is much lower in lower mammals, perhaps providing a partial answer to the question of what makes the human brain "human" [5,8].
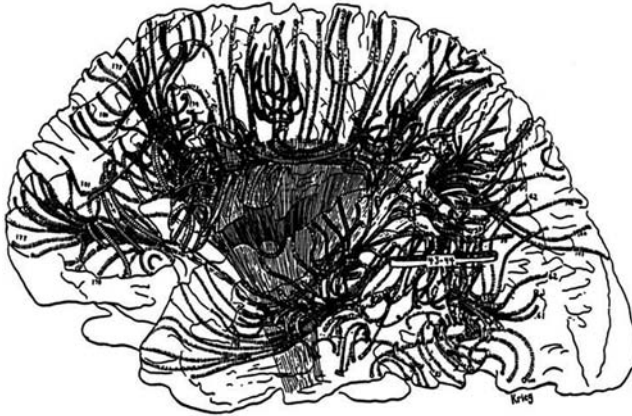
Figure 6.3 A few of the 10^{10} corticocortical (white matter) fibers obtained by physical dissection from a postmortem human brain [7,30,31].

The actual corticocortical fibers shown in Figure 6.3 were physically dissected from a postmortem human brain [30,31];. modern studies estimate fiber tracks using diffusion tensor imaging [9]. Cerebral cortex is divided into 50 Brodmann areas, based on relatively minor differences in cell layers and structures, which in some cases are known to correspond to distinct physiological functions, for example, in visual, auditory, somatosensory, and motor cortex. The 10^{10} corticocortical fibers are sufficiently numerous to allow every macrocolumn to be connected to every other macrocolumn in an idealized homogeneous system. Because of connection specificity (some columns more densely interconnected than others), full interconnectivity occurs at a somewhat larger scale, but probably less than 1 cm.

While specificity of fiber tracts prevents full connectivity at the macrocolumn scale, any pair of cortical neurons is typically separated by a *path length* of no more than two or three synapses. The corticocortical network's path length is analogous to the global human social network with its so-called *six degrees of separation* between any two humans. Small world phenomena are studied in *graph theory* and also appear widely in physical, social [10], and brain [9] systems.

6.3
Multiscale Theory in Electrophysiology

6.3.1
Characteristic EEG and Physiological Time Scales

This chapter aims to provide a tentative, but physiologically based theoretical framework for experimental observations of brain dynamics with emphasis on the large-scale (centimeter) extra cranial electric field (EEG). Since the first human

recording in the early 1920s, the physiological basis for the wide range of rhythmic EEG activities, a proverbial "spectral zoo," has been somewhat of a mystery [7,8,18]. In particular, human alpha rhythms, which are robust in awake and relaxed subjects with closed eyes, may be recorded over nearly all of the upper scalp or cortex and have preferred frequencies near 10 Hz. Given any unknown system that produces oscillations at some preferred (or resonant) frequency $f = \omega/2\pi$, an obvious question concerns the origin of the underlying time scale

$$\tau \sim \omega^{-1}. \tag{6.1}$$

The implied physiological time scales for the most robust human EEG rhythms (1–15 Hz) are $\tau = 10$–160 ms. How does this delay range compare with mammalian physiology? Whereas early studies of membrane time constants were typically less than 10 ms, more modern studies with improved recording methods report the wide range 20–100 ms [32]. But in voltage-gated membrane ion channels, the effective time constant becomes a "dynamical parameter" that depends on both membrane voltage and time, thus genuine time constants are not really "constant." Koch *et al.* [32] argue that the voltage response to very brief synaptic inputs is essentially independent of the classically defined time constant. These studies suggest that while synaptic delays (PSP rise and decay times) lie within an order of magnitude of dominant EEG time scales, claims of close agreement between the details of observed EEG spectra and dynamic theories, based only on membrane time constants, are not credible. Model parameters can be chosen to "match" favored EEG data sets, which, in any case, can vary widely between individuals and brain states.

In contrast to these *local delays* at the single neuron level, *global* propagation delays along the longest corticocortical fibers are roughly in the 30 ms range in humans [7,15]. Such global delays depend on axon length and propagation speed distributions. While both local and global delays appear to be in a general range to account for oscillatory EEG dynamics, this semiquantitative observation fails to explain the physiological mechanisms responsible for "special frequencies" like the narrow band human alpha rhythms or gamma oscillations (≈40 Hz), the latter recorded mostly from inside the craniums of humans and lower mammals. Nevertheless, we can search for qualitative and semiquantitative connections between theory and EEG experiments that do not require precise physiological parameter knowledge.

6.3.2
Local versus Global Brain Models and Spatial Scale

To distinguish complementary theories of neocortical dynamics, we employ the label *local theory* to indicate mathematical models of cortical or thalamocortical interactions for which corticocortical axon propagation delays are assumed to be zero [8,15]. The underlying time scales in these theories typically originate from membrane time constants, essentially the resistive–capacitive responses of neural membranes to local synaptic input. Thalamocortical networks are also "local" from the viewpoint of surface electrodes, which cannot distinguish purely cortical from

thalamocortical networks. Finally, these theories are "local" in the sense of being independent of global boundary conditions.

By contrast, *global theory* indicates mathematical models in which delays in corticocortical fibers provide the underlying time scales for the large-scale EEG dynamics recorded by scalp electrodes. Periodic boundary conditions are generally essential to global theories because the cortical white matter system is topologically close to a spherical shell. While this picture of distinct local and global models greatly oversimplifies expected genuine dynamic behaviors with substantial cross-scale interactions, it also provides a convenient entry point to brain complexity.

6.3.3
A Large-Scale Model of EEG Standing Waves

Given the large volume of experimental EEG data involving frequency spectra, synchrony, coherence, covariance, and so forth, we first consider a large-scale model developed specifically to explain observed EEG dynamic behavior in terms of the underlying physiology and anatomy, mostly independent of behavioral and cognitive issues. The general idea of standing EEG waves [5,7,14,15,17] is based on the following simple idea: Nature's ubiquitous standing waves occur when the traveling waves of some *field* interact to produce *interference* (adding together); that is, when positive and negative fields meet and tend to cancel each other. For example, the up and down displacements of a violin string from its resting position may be represented as a field. Waves in the string traveling in opposing directions interfere (add together) to produce standing waves. More generally, a "field" may represent nearly any physical quantity. In the case of brain waves, the proposed fields consist of the numbers of active inhibitory and excitatory synapses in each (centimeter scale) tissue mass. These synaptic fields differ from the electric and magnetic fields that they produce.

Nearly any kind of weakly damped wave phenomenon propagating in a medium with characteristic speed v is expected to produce standing waves due to wave interference that depends on the system's boundary conditions (forcing traveling waves to combine). For example, wave interference in neural tissue may be expected due to cancellation of excitatory and inhibitory synaptic action fields in macroscopic (millimeter to centimeter scale) tissue masses. Interference and the attendant standing waves also occur in violin strings, electric systems, quantum wave functions, and numerous other vibrating mechanical, electrical, chemical, and biological systems.

Whereas waves in strings and flutes are reflected from boundaries, waves in closed systems like spherical shells or tori interfere because of periodic boundary conditions causing waves traveling in opposing directions to meet and combine. As a result of this interference, preferred (resonant) frequencies persist in such systems. Examples of standing waves in spherical geometry include the quantum wave function of the hydrogen atom (both radial and tangential waves), and the Schumann resonances of electromagnetic waves in the spherical shell formed by the earth's surface and the bottom of the ionosphere (tangential waves only) [33].

The lowest frequency, often dominant in such systems, is the fundamental mode. This fundamental frequency is given for the geometries of a spherical shell of radius R or a one-dimensional loop of length $L = 2\pi R$, perhaps closed loops of transmission line or stretched string [7], by

$$f = \frac{g\nu}{L}. \tag{6.2}$$

Here, the geometric constant g is either $\sqrt{2}$ (spherical shell) or 1 (one-dimensional loop). Each cortical hemisphere together with its white matter connections is topographically essentially a spherical shell. On the contrary, the postulated medium characteristic speed ν is the axon propagation speed in the longer systems of corticocortical axons forming in the white matter layer. Since these fibers may be substantially anisotropic with a preferred anterior–posterior orientation, it is unclear whether the shell or loop model is the most appropriate.

The wrinkled surface of each cortical hemisphere can be reshaped or mentally inflated (as with a balloon) to create an equivalent spherical shell with effective radius R related to its surface area by the relation

$$R = \sqrt{\frac{A}{4\pi}}. \tag{6.3}$$

Thus, cerebral cortex and its white matter system of (mostly) corticocortical fibers is a system somewhat analogous to the earth–ionosphere shell. With a brain hemispheric surface area $A \approx 800-1500\,\text{cm}^2$, or alternately an anterior–posterior closed cortical loop of $L \approx 50-70\,\text{cm}$ (ellipsoid-like circumference), and a characteristic cortico-cortical axon propagation speed of $\nu \approx 600-900\,\text{cm/s}$ [7,8,17,18], the predicted fundamental cortical frequency predicted by naive application of Equation 6.2 is then

$$f \approx 8-26\,\text{Hz}. \tag{6.4}$$

We call this estimate "naive" because the fundamental mode frequency depends on both the physical shape and material properties of the wave medium (cortex-white matter). These latter properties determine the dispersive nature of the waves; that is, the precise manner in which the waves of synaptic activity distort when propagating. Such dispersive properties in cortex must depend on the nature and interactions of the synaptic and action potential fields. Furthermore, cortical frequency must depend on at least one additional parameter determined by brain state. Thus, estimates in Equations 6.2 and 6.4 cannot be expected to represent genuine brain waves, even if the cortex were actually a spherical shell or closed loop, the postulated brain waves are much more likely to be dispersive (if for no other reason than most of Nature's waves are dispersive). Furthermore, the expected neural networks of cognitive processing (believed to be embedded in global synaptic wave fields) are expected to cloud experimental observations of standing wave phenomenon. One may guess that such networks involve thalamocortical interactions that can generate preferred frequencies in several bands, including alpha (near 10 Hz) and gamma (near 40 Hz). Thus, scalp potentials seem to consist of a mixture of interacting global and local activities, both of which underlie and are correlated with cognitive processing.

This general picture does not, in itself, constitute a brain theory; rather it simply suggests a hypothesis and related experiments to test for *traveling* and *standing brain waves* of synaptic activity. If estimate Equation 6.4 had been obtained before the discovery of the human alpha rhythm, it would have provided a plausible and testable prediction. One appropriate experimental question would have been, "Can brain states be found in which neural network activity is sufficiently suppressed to allow observation of relatively simple standing waves?" Such imagined experiments would have found the predicted EEG oscillations in the 8–13 Hz band in relaxed subjects (minimal mental load implying minimal network activity) with closed eyes (minimal visual processing). The genuine (physiologically based) neocortical standing wave theory, its relationships to local theories, and multiple experimental implications have been presented in a series of papers over the past 40 years [7,8,14–18]. Experimental connections to issues of myelin maturation, axon propagation speed, brain size, traveling and standing EEG waves, phase and group velocities, and so forth are summarized in several references [5,7,8,15–18]. Since mathematical derivation of this brain theory has been widely published earlier, we here replace the genuine brain theory with the simple analog mechanical system of Section 6.3.4 in order to emphasize the independence of our general conceptual framework from model specifics.

6.3.4
Relationships between Small, Intermediate, and Large Scales: A Simple Mechanical Analog

Brain dynamic behavior, including EEG, is apparently due to some combination of global and local processes with important top-down and bottom-up interactions across spatial scales, that is, circular causality. In treating global mechanisms, we stress the importance of myelinated axon propagation delays and periodic boundary conditions in the cortical-white matter system. By contrast, proposed local mechanisms are multiscale interactions between cortical columns via short-ranged (intracortical) nonmyelinated fibers. We first propose this general picture as an essential conceptual framework, which is demonstrated with both metaphorical systems and outlines of genuine theories developed at macroscopic and mesoscopic scales.

In order to introduce the (macroscopic scale) standing wave theory of Section 6.3 and its relationship to the mesoscopic (statistical mechanical) theory of Section 6.4, we offer a simple mechanical analog consisting of a closed loop of stretched string with attached subsystems, as shown in Figure 6.4 [7,12,34]. The imagined subsystems might be anything from the simple linear springs drawn in Figure 6.4 to complex, multiscale nonlinear systems (not shown). In the case of minimal (bottom-up) influences from the subsystems, the string produces standing waves analogous to both the large-scale coherent EEG observed in several brain states and the genuine global brain model outlined in Section 6.3.3. Actual and observed string amplitudes are given by $\Phi(x, t)$ and $\hat{\Phi}(x, t)$, respectively; the latter representing a spatial low-pass version of the former due to a "blurring layer" analogous to the skull and other
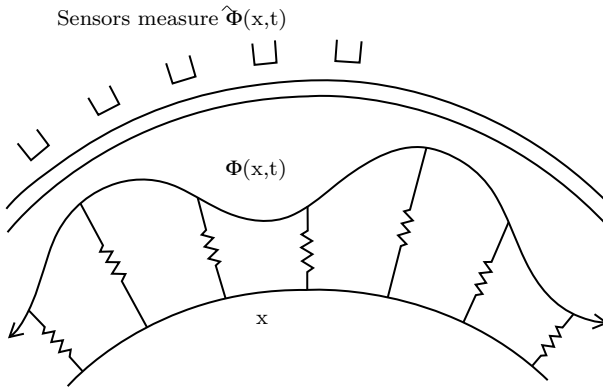
Figure 6.4 Mechanical cortical analog consisting of a closed loop of stretched string with attached subsystems, shown here as simple mechanical springs [7,12,34]. Actual string displacement is given by $\Phi(x,t)$, analogous to brain surface (ECoG) recordings. The spatial low-pass (experimental) observable is given by $\hat{\Phi}(x,t)$, analogous to scalp (EEG) recordings.

intervening tissues. EEGs, recorded from the brain and scalp, are analogous to $\Phi(x,t)$ and $\hat{\Phi}(x,t)$, respectively. The attached subsystems serve as analogs for smaller (mesoscopic) scale columnar dynamics of neocortex. Generally, we expect string displacement and EEG at all scales to result from global and local phenomena, acting both top down and bottom up, demonstrating a robust circular causality associated with synergetics [4,35].

The proposed metaphorical relationships of string and springs to neocortex are outlined in Table 6.3. String displacement Φ is governed by the basic string equation

$$\frac{\partial^2 \Phi}{\partial t^2} - v^2 \frac{\partial^2 \Phi}{\partial x^2} + \left[\omega_0^2 + f(\Phi) \right] \Phi = 0. \tag{6.5}$$

In the simple case of homogeneous linear springs, string of length L (forming a closed loop), and wave propagation speed v (determined by string tension and mass), $f(\Phi) = 0$, and the normal modes (resonant frequencies) of standing waves are given by

$$\omega_n^2 = \omega_0^2 + \left(\frac{n\pi v}{L} \right)^2, \quad n = 2, 4, 6, \ldots. \tag{6.6}$$

In this simple limiting case, the natural oscillation frequencies are seen as having distinct local and global contributions given by the first and second terms, respectively, on the right side of Equation 6.6. This same dispersion relation occurs for waves in hot plasmas and transmission lines; the latter might also form a closed loop analogous to cortical topology and the periodic boundary

Table 6.3 The string–springs analog.

Closed loop of stretched string	Neocortex/white matter axons
String displacement $\Phi(x, t)$	Any cortical field (synaptic, firing density, etc.)
String wave speed v	Corticocortical axon speed
Spring natural frequency ω_0	Simple local corticothalamic network
Nonlinear stiffness effect $\omega_0^2 + f[\Phi(x, t)]$	Multiscale nonlinear effects generated at columnar scales
Relax string tension $v \rightarrow 0$	Ignore axon delays
Disconnect boxes (springs) $\omega_0, f[\Phi(x, t)] \rightarrow 0$	Ignore local dynamics

condition, appropriate for cortical standing waves [7,8,15]. If the springs are disconnected from the string, only the global dynamics remain as indicated in Table 6.3. In the opposite limit where string tension is relaxed, only the local dynamics remain. In actual brains, both local and global extremes and everything in between are expected in various brain states controlled by neurotransmitters [2,5,9,35]. The relaxed (eyes closed) alpha state and several anesthesia states may be examples of dominant global dynamics, analogous to disconnected springs. By contrast, diseases like *schizophrenia* might provide examples of extreme dynamic isolation, with each brain region doing its own thing, thereby failing to provide a unified consciousness [27], states analogous to relaxed tension in the mechanical string analog.

In Section 6.4, the nonlinear cortical system is modeled such that local and global effects are integrated through a process analogous to the nonlinear spring function $f(\Phi)$. This approach to neuroscience is based on neocortical evolution in which neural minicolumns interact via short-ranged fibers in macrocolumns and by means of long-ranged interactions across regions of macrocolumns. This common architecture processes patterns of information within and among different regions; that is, in sensory, motor, associative cortex, and so forth. In order to satisfy space constraints but still remain faithful to genuine brain physics and physiology, the presentation of Section 6.4 retains only essential technical detail.

6.4
Statistical Mechanics of Neocortical Interactions

6.4.1
SMNI on Short-Term Memory and EEG

A SMNI for human neocortex has been developed, building from synaptic interactions to minicolumnar, macrocolumnar, and regional interactions in neocortex [11,19]. Over a span of approximately 30 years, a series of about 30 papers on SMNI

has been developed to model columns and regions of neocortex, spanning millimeter to centimeter scales of tissue.

SMNI develops three biophysical scales of neocortical interactions: microscopic neurons [36], mesocolumnar domains [37], and macroscopic regions. SMNI has developed conditional probability distributions at each level, aggregating up to several levels of interactions. Synaptic interneuronal interactions, averaged over by mesocolumns, are phenomenologically described by the mean and variance of a distribution Ψ (both Poisson and Gaussian distributions are considered, giving similar results). Similarly, intraneuronal transmissions are phenomenologically described by the mean and variance of Γ (a Gaussian distribution).

Mesocolumnar averaged excitatory (*E*) and inhibitory (*I*) neuronal firings *M* are followed. The vertical organization of minicolumns, with their horizontal stratification, yields a physiological entity, the mesocolumn. This reflects on typical individual neuronal refractory periods of about 1 ms, during which another action potential cannot be initiated, and a relative refractory period of 0.5–10 ms. Macroscopic regions of neocortex are depicted as arising from many mesocolumnar domains, with regions coupled by long-ranged interactions.

Most of these papers have dealt explicitly with calculating properties of short-term memory (STM) and scalp EEG in order to test the basic formulation of this approach [11,12,19,20,38–43]. The SMNI modeling of local mesocolumnar interactions that is calculated to include convergence and divergence between minicolumnar and macrocolumnar interactions was tested on established STM phenomena. The SMNI modeling of macrocolumnar interactions across regions was tested on EEG. The EEG studies in SMNI applications were focused on regional scales of interactions, as well as on columnar scales of interactions.

6.4.1.1 **SMNI STM**

SMNI studies have detailed that maximal numbers of attractors lie within the physical firing space of M^G, where $G = \{\text{excitatory, inhibitory}\} = \{E, I\}$ minicolumnar firings, consistent with experimentally observed capacities of auditory and visual short-term memory, when a Centering Mechanism is enforced by shifting background noise in synaptic interactions, consistent with experimental observations under conditions of selective attention [40,43–45]. This leads to all attractors of the short-time distribution lying approximately along a diagonal line in M^G space, effectively defining a narrow parabolic trough containing these most likely firing states. This essentially collapses the two-dimensional M^G space down to a one-dimensional space of primary importance. Thus, the predominant physics of STM and of (short-fiber contribution to) EEG phenomena takes place in this narrow parabolic trough in M^G space, roughly along a diagonal line.

These calculations were further supported by high-resolution evolution of the short-time conditional probability propagator using a numerical path-integral

code, PATHINT [43]. SMNI correctly calculated the stability and duration of STM, the observed 7 ± 2 capacity rule of auditory memory and the observed 4 ± 2 capacity rule of visual memory [45–47], the primacy versus recency rule, random access to memories within tenths of a second as observed, and Hick's law of linearity of reaction time with STM information [48–50]. SMNI also calculates how STM patterns (e.g., from a given region or even aggregated from multiple regions) may be encoded by dynamic modification of synaptic parameters (within experimentally observed ranges) into long-term memory (LTM) pattern [19].

6.4.1.2 SMNI EEG

Using the power of this formal mathematical structure, sets of EEG and evoked potential data from a separate NIH study, collected to investigate genetic predispositions to alcoholism, were fitted to an SMNI model on a lattice of regional electrodes to extract brain signatures of STM [41]. Each electrode site was represented by an SMNI distribution of independent stochastic macrocolumnar-scaled M^G variables, interconnected by long-ranged circuitry with delays appropriate to long-fiber communication in neocortex. The global optimization algorithm adaptive simulated annealing (ASA) [51] was used to perform maximum likelihood fits of Lagrangians defined by path integrals of multivariate conditional probabilities. Canonical momenta indicators, the momentum components of the Euler–Lagrange equations discussed below, were thereby derived for individual's EEG data. These indicators give better signal recognition than the raw data, and were used as correlates of behavioral states. In-sample data was used for training [41], and out-of-sample data was used for testing these fits.

These results gave quantitative support for an accurate intuitive picture, portraying neocortical interactions as having common algebraic physics mechanisms that scale across quite disparate spatial scales and functional or behavioral phenomena; that is, describing interactions among neurons, columns of neurons, and regional masses of neurons.

6.4.2
Euler–Lagrange Equations

To investigate the dynamics of multivariate stochastic nonlinear systems, such as neocortex, it is often not sensible to apply simple mean-field theories that assume sharply peaked distributions, since the dynamics of nonlinear diffusions in particular are typically washed out. Here, path integral representations of systems, otherwise equivalently represented by Langevin or Fokker–Planck equations, present elegant algorithms by use of variational principles leading to Eular–Lagrange (EL) equations [52]. Explicit calculations were performed over the evolution of these probability distributions [43]. SMNI also permits scaling to derive EL in several approximations, which give insight into other phenomena that take advantage of the SMNI STM approach.

6.4.2.1 Columnar EL

The Lagrangian components and EL equations are essentially the counterpart to classical dynamics

$$
\text{Mass} = g_{GG'} = \frac{\partial^2 L}{\partial(\partial M^G/\partial t)\partial(\partial M^{G'}/\partial t)},
$$

$$
\text{Momentum} = \Pi^G = \frac{\partial L}{\partial(\partial M^G/\partial t)},
$$

$$
\text{Force} = \frac{\partial L}{\partial M^G},
$$

$$
\text{F-ma} = 0 : \delta L = 0 = \frac{\partial L}{\partial M^G} - \frac{\partial}{\partial t}\frac{\partial L}{\partial(\partial M^G/\partial t)}. \tag{6.7}
$$

Concepts such as momentum, force, inertia, are so ingrained into our culture, that we apply them to many stochastic systems, such as weather, financial markets, and others, often without giving much thought to how these concepts might be precisely identified. For a large class of stochastic systems, even including nonlinear non-equilibrium multivariate Gaussian–Markovian systems like SMNI, the above formulation is precise. That is, the means and covariances (first and second moments) of the probability distributions defined in Equation 6.8 below are necessary and sufficient to calculate all the above dynamical variables in Equation 6.7 above.

The EL equations are derived from the long-time conditional probability distribution of columnar firings over all cortexes, represented by $\tilde{M}$, in terms of the Action S,

$$
\tilde{P}[\tilde{M}(t)]\mathrm{d}\tilde{M}(t) = \int \ldots \int D\tilde{M}\exp(-N\tilde{S}),
$$

$$
\tilde{M} = \{M^{G\nu}\}, \quad \tilde{S} = \int_{t_0}^{t}\mathrm{d}t'\tilde{L}, \quad \tilde{L} = \Lambda\Omega^{-1}\int \mathrm{d}^2 rL, \quad L = L^E + L^I, \tag{6.8}
$$

$$
D\tilde{M} = \prod_{s=1}^{u+1}\prod_{\nu=1}^{\Lambda}\prod_{G}^{E,I}(2\pi\,\mathrm{d}t)^{-1/2}(g_s^\nu)^{1/4}\,\mathrm{d}M_s^{G\nu}\delta[M_t = M(t)]\delta[M_0 = M(t_0)],
$$

where ν labels the two-dimensional laminar r space of $\Lambda \approx 5\times 10^5$ mesocolumns spanning a typical region of neocortex, Ω, (total cortical area $\approx 4\times 10^{11}\,\mu\text{m}^2$); and s labels the $u+1$ time intervals, each of duration $\mathrm{d}t \leq \tau$, spanning $(t - t_0)$. At a given value of $(r;t)$, $M = \{M^G\}$.

The path integral has a variational principle, $\delta L = 0$ that yields the EL equations for SMNI [9,10]. Linearization of the EL equations permits the development of stability analyses and dispersion relations in frequency–wave number space [11,19,53], leading to wave propagation velocities of interactions over several minicolumns, consistent with the intermediate scale of cortical recordings. This calculation first linearizes the EL, then takes Fourier transforms in space and time variables.

For instance, a typical example [51] yields (dispersive) dispersion relations

$$
\omega\tau = \pm\{-1.86 + 2.38(\xi\rho)^2; -1.25i + 1.51i(\xi\rho)^2\}, \tag{6.9}
$$

where ξ is the wave number. The propagation velocity defined by $d\omega/d\xi$ is about 1 cm/s, taking a typical ξ to correspond to macrocolumnar distances of about 30ρ. Calculated frequencies ω are on the order of EEG frequencies of about $10^2\,\mathrm{s}^{-1}$. These mesoscopic propagation velocities permit processing over several minicolumns about $10^{-1}\,\mathrm{cm}$, simultaneous with processing of mesoscopic interactions over tens of centimeters via association fibers with propagation velocities about 600–900 cm/s; that is, both can occur within about $10^{-1}\,\mathrm{s}$. Note that this propagation velocity is not "slow": Visual selective attention moves at about $8\,\mathrm{ms}/°$, which is about $1/2\,\mathrm{mm/s}$ if a macrocolumn of about mm^2 is assumed to span $180°$. This suggests that nearest-neighbor interactions play some part in disengaging and orienting selective attention.

6.4.2.2 Strings EL

The nonlinear string model was derived using the EL equation for the electric potential Φ recorded as EEG, considering one firing variable along the parabolic trough of attractor states being proportional to Φ [54]. Since only one variable, the electric potential is being measured; it is reasonable to assume that a single independent firing variable offers a crude description of this biophysics. Furthermore, the scalp potential Φ can be considered to be a function of this firing variable. In an abbreviated notation subscripting the time dependence

$$\Phi_t - \langle\Phi\rangle = \Phi(M_t^E, M_t^I) \approx a(M_t^E - \langle M^E\rangle) + b(M_t^I - \langle M^I\rangle), \tag{6.10}$$

where a and b are constants, and $\langle\Phi\rangle$ and $\langle M^G\rangle$ represent typical minima in the trough. In the context of fitting data to the dynamic variables, there are three effective constants, $\{a, b, \phi\}$

$$\Phi_t - \phi = aM_t^E + bM_t^I. \tag{6.11}$$

The mesoscopic columnar probability distributions P_Φ is scaled over this columnar firing space to obtain the macroscopic conditional probability distribution over the scalp-potential space

$$P_\Phi[\Phi] = \int dM^E\, dM^I P[M^E, M^I]\delta[\Phi - \Phi'(M^E, M^I)]. \tag{6.12}$$

The parabolic trough described above justifies a form

$$\begin{aligned} P_\Phi &= (2\pi\sigma^2)^{-1/2}\exp(-\Delta t\int dx L_\Phi),\\ L_\Phi &= \frac{\alpha}{2}\left|\frac{\partial\Phi}{\partial t}\right|^2 + \frac{\beta}{2}\left|\frac{\partial\Phi}{\partial x}\right|^2 + \frac{\gamma}{2}|\Phi|^2 + F(\Phi),\\ \sigma^2 &= \frac{2\Delta t}{\alpha}. \end{aligned} \tag{6.13}$$

Here $F(\Phi)$ contains nonlinearities away from the trough, σ^2 is on the order of $1/N$ given the derivation of L_Φ above, and the integral over x is taken over the spatial region of interest. In general, there also will be terms linear in $\partial\Phi/\partial t$ and $\partial\Phi/\partial x$. There exist regions in neocortical parameter space such that the nonlinear string model is recovered. Note that if the spatial extent is extended across the scalp via long-ranged fibers connecting columns with $M^{\ddagger E'}$ firings, this leads to a string of columns.

6.4.2.3 Springs EL

For a given column in terms of the probability description given above, the above EL equations are represented as

$$\frac{\partial}{\partial t}\frac{\partial L}{\partial(\partial M^E/\partial t)} - \frac{\partial L}{\partial M^E} = 0,$$

$$\frac{\partial}{\partial t}\frac{\partial L}{\partial(\partial M^I/\partial t)} - \frac{\partial L}{\partial M^I} = 0. \tag{6.14}$$

Previous studies on SMNI EEG had demonstrated that simple linearized dispersion relations, derived from the EL equations, support the local generation of frequencies observed experimentally, as well as deriving diffusive propagation velocities of information across minicolumns consistent with other experimental studies. The above equations can then also represent coupled springs. The earliest studies simply used a driving force $J_G M^G$ in the Lagrangian to model long-ranged interactions among fibers [11,19]. Subsequent studies considered regional interactions driving localized columnar activity within these regions [41,55].

A set of calculations examined these columnar EL equations to see if EEG oscillatory behavior could be supported at just this columnar scale, that is, within a single column. The EL equations were quasilinearized, by extracting coefficients of M and dM/dt. This exercise demonstrated that a spring-type model of oscillations was plausible. A more detailed study was then performed, developing over 2 million lines of C code from the algebra generated by the algebraic tool Maxima to see what range of oscillatory behavior could be considered as optimal solutions, satisfying the EL equations [56]. These results survive even with oscillatory input into minicolumns from long-ranged sources [12], since the Centering Mechanism is independent of firing states, and depends only on averaged synaptic values used in SMNI.

6.4.3
Smoking Gun

As yet, there does not seem to be any "smoking gun" for explicit top to down mechanisms that directly drive bottom-up STM processes. Of course, there are many top-down type studies demonstrating that neuromodulator [27] and neuronal firing states (defined by EEG, for example) can modify the milieu or context of individual synaptic and neuronal activity, which is still consistent with ultimate

bottom-up paradigms. However, there is a logical difference between top-down milieu as conditioned by some prior external or internal conditions, and some direct top-down processes that directly cause bottom-up interactions, specific to STM. Here, the operative word is "cause."

6.4.3.1 Neocortical Magnetic Fields

There are many studies on electric [57] and magnetic fields in neocortex [54,58,59]. At the level of single neurons, electric field strengths can be as high as about $10\,\text{V/m}$ for a summation of excitatory or inhibitory postsynaptic potentials as a neuron fires. The electric field $\mathbf{D} = \varepsilon\mathbf{E}$ is rapidly attenuated as the dielectric constant ε seen by ions is close to two orders of magnitude than ε_0 (vacuum), due to polarization of water just outside the neuron [8,15]. Magnetic field strengths $\mathbf{H}$ in neocortex are generally quite small, even when estimated for the largest human axons at about 10^{-7}T, roughly $1/300$ of the Earth's magnetic field, based on ferrofluid approximation to the microtubule environment with a magnetic permeability μ, $\mathbf{B} = \mu\mathbf{H}$, about $10\mu_0$ [58]. Thus, the electromagnetic fields in neocortex differ substantially from those in vacuum. These estimates of magnetic field strengths appear to be reliable when comparisons between theoretical and experimental measurements are made in crayfish axons [54].

The above estimates of electric and magnetic field strengths do not consider collective interactions within and among neighboring minicolumns, which give rise to much larger field strengths as typically measured by noninvasive EEG and MEG recordings. While electrical activity may be attenuated in the neocortical environment, this is not true for magnetic fields, which may increase collective strengths over relatively large neocortical distances. The strengths of magnetic fields in neocortex may be at a threshold to directly influence synaptic interactions with astrocytes, as proposed for LTM [60] and STM [61,62]. Magnetic strengths associated with collective EEG activity at a columnar level gives rise to even stronger magnetic fields. Columnar excitatory and inhibitory processes largely take place in different neocortical laminae, providing possibilities for more specific mechanisms.

6.4.3.2 SMNI Vector Potential

To demonstrate that top-down influences can be appreciable, a direct comparison was described between the momentum $\mathbf{p}$ of Ca^{2+} ions, which have been established as being influential in STM and LTM, and an SMNI vector potential (SMNI-VP) [63,64]. The SMNI-VP is constructed from magnetic fields induced by neuronal electrical firings at thresholds of collective minicolumnar activity with laminar specification, and can give rise to causal top-down mechanisms that effect molecular excitatory and inhibitory processes in STM and LTM. A specific example might be the causal influences on momentum $\mathbf{p}$ of Ca^{2+} ions by the SMNI-VP $\mathbf{A}$, as calculated by the canonical momentum $\mathbf{q} = \mathbf{p} - e\mathbf{A}$, where e is the electron coulomb charge and $\mathbf{B} = \nabla \times \mathbf{A}$ is the magnetic field, which may be applied either classically or quantum mechanically. Note that gauge of $\mathbf{A}$ is not specified here, and this can lead to important effects especially at quantum scales.

The comparison of **p** and **A** demonstrates that it is possible for minicolumnar electromagnetic fields to influence important ions involved in cognitive and affective processes in neocortex [63,64]. The estimate of the minicolumnar electric dipole is quite conservative, and a factor of 10 would make these effects even more dramatic. Since this effect acts on all Ca^{2+} ions, it may have an even greater effect on Ca^{2+} waves, contributing to their mean wave front movement. Considering slower ion momentum **p** would make this comparison to **A** even closer. Such a smoking gun for top-down effects awaits forensic *in vivo* experimental verification, requiring appreciating the necessity and due diligence of including true multiscale interactions across orders of magnitude, in the complex neocortical environment.

6.5
Concluding Remarks

We have outlined how human consciousness and its behavioral consequences are strongly correlated with the dynamic behaviors of several kinds of brain processes, observed at distinct spatial and temporal scales. fMRI and PET track local blood oxygen and metabolic activity, respectively, obtaining good spatial resolution (millimeter) and intermediate-scale temporal resolution (seconds to minutes). By contrast, scalp EEG provides extra cranial electric field patterns with temporal resolution (millisecond) faster than the speed of thought [5], but very coarse (2–10 cm) spatial resolution. Most experimental and theoretical studies emphasize cerebral cortex, the structure producing nearly all recordable scalp potentials, and believed to be directly responsible for much of conscious experience.

Brains are often viewed as the preeminent complex systems with consciousness emerging from dynamic interactions within and between brain subsystems. The emergence of novel features in complex systems is expected to depend critically on cross-scale interactions, where dynamic variables interact both top-down and bottom-up, for example, at the multiple columnar scales of cortical tissue. Our experimental discussions focus on EEG, which over the past 80 years has provided nearly all the millisecond scale data associated with consciousness, providing important quantitative measures of medical conditions such as epilepsy and coma, as well as task performances involving attention, mental calculations, and so forth. Another interesting category of EEG work employs binocular rivalry, in which inputs from two distinct visual images enter the brain simultaneously, but reach the level of conscious awareness only one image at a time. The EEG and other data provide many neural correlates of consciousness, including measures of functional connections between brain regions, for example, covariance in the time domain and coherence in the frequency domain.

For the past century or so the Holy Grail of neuroscience has been the connection of anatomy and physiology to psychology. In this chapter, we suggest approaching this goal in two stages: Connect the anatomy/physiology to experimental EEG by employing brain theory. Then examine the various conscious correlates of these data. In the first step, we outlined a global EEG model that stresses myelinated

axon propagation delays and periodic boundary conditions in the cortical-white matter system. As this system is topologically close to a spherical shell, standing waves of synaptic action fields are predicted with fundamental frequency in the typical EEG range near 10 Hz. The genuine neural model, in contrast to the mechanical analog of this chapter, provides experimental connections to issues of myelin maturation, axon propagation speed, brain size, traveling and standing waves observed on the scalp, phase and group velocities, and other aspects of very large-scale (2–10 cm) brain dynamics. These experimental connections generally tend to support the standing wave theory.

In contrast to the purely global model, the proposed local mechanisms are multiscale interactions between cortical columns via short-ranged nonmyelinated fibers. A SMNI predicts oscillatory behavior within columns, between neighboring columns and via short-ranged nonmyelinated fibers. The columnar dynamics, based partly on membrane time constants, also predicts frequencies in the range of EEG. We generally expect both local and global processes to influence EEG at all scales, including the very large-scale scalp data. Thus, SMNI also includes interactions across cortical regions via myelinated fibers effecting coupling of local and global models. In order reach a wider audience, the combined local–global dynamics is demonstrated with an analog mechanical system consisting of a stretch string (producing standing waves analogous to those of the global neural model) with attached nonlinear springs (representing columnar dynamics). SMNI is able to derive a string equation consistent with the analog global model.

To summarize this chapter, we have outlined plausible relationships between physiology/anatomy and its attendant dynamic behavior to other complex systems. We provided brain experimental data obtained at multiple spatial and temporal scales. Based on this background, we then proposed a dynamic conceptual framework, largely independent of theoretical details, consisting of columnar dynamics embedded in a global standing wave environment of synaptic activity. Such framework can support future experimental and theoretical studies of neocortical interactions and their associated dynamics. By employing this conceptual framework we have directly addressed the first basic question of this chapter, that is, "What are the *neural correlates* of consciousness?" Furthermore, we have suggested several tentative answers to the second basic question, "What are the *necessary conditions* for consciousness?" Such answers are closely involved with various aspects of multiscale brain complexity. The third basic question concerning the *sufficient conditions* for consciousness to occur remains a deep black hole of ignorance.

References

1 Mountcastle, V. (1998) *Perceptual Neuroscience: The Cerebral Cortex*, Harvard University Press, Cambridge.

2 Edelman, G.M. and Tononi, G. (2000) *A Universe of Consciousness*, Basic Books, New York.

3 Bassett, D.S. and Gazzaniga, M.S. (2011) Understanding complexity in the human brain. *Trends Cogn. Sci.*, **15**, 200–209.

4 Haken, H. (1996) *Principles of Brain Functioning: A Synergetic Approach to Brain*

Activity, Behavior, and Cognition, Springer, Berlin.

5 Nunez, P.L. (2010) *Brain, Mind, and the Structure of Reality*, Oxford University Press, New York.

6 Feinberg, T.E. (2012) Neuroontology, neurobiological naturalism, and consciousness: a challenge to scientific reduction and a solution (including commentaries by author PLN and others). *Phys. Life Rev.*, **9**, 13–46.

7 Nunez, P.L. (1995) *Neocortical Dynamics and Human EEG Rhythms*, Oxford University Press, New York.

8 Nunez, P.L. and Srinivasan, R. (2006) *Electric Fields of the Brain: The Neurophysics of EEG*, 2nd edn, Oxford University Press, New York.

9 Sporns, O. (2011) *Networks of the Brain*, MIT Press, Cambridge.

10 Watts, D.J. (1999) *Small Worlds*, Princeton University Press, Princeton.

11 Ingber, L. (1982) Statistical mechanics of neocortical interactions. I. Basic formulation. *Physica D*, **5**, 83–107.

12 Ingber, L. and Nunez, P.L. (2010) Neocortical dynamics at multiple scales: EEG standing waves, statistical mechanics, and physical analogs. *Math. Biosci.*, **229**, 160–173.

13 Chalmers, D.L. (2010) *The Character of Consciousness*, Oxford University Press, New York.

14 Nunez, P.L. (1974) The brain wave equation: a model for the EEG. *Math. Biosci.*, **21**, 279–297, First presented to American EEG Society Meeting, Houston, 1972.

15 Nunez, P.L. (1989) Generation of human EEG by a combination of long and short range neocortical interactions. *Brain Topogr.*, **1**, 199–215.

16 Nunez, P.L. (2000) Toward a quantitative description of large scale neocortical dynamic behavior and EEG. *Behav. Brain Sci.*, **23**, 371–437.

17 Nunez, P.L. and Srinivasan, R. (2006) A theoretical basis for standing and traveling brain waves measured with human EEG with implications for an integrated consciousness. *Clin. Neurophysiol.*, **117**, 2424–2435.

18 Nunez, P.L. (2011) Implications of white matter correlates of EEG standing and traveling waves. *Neuroimage*, **57**, 1293–1299.

19 Ingber, L. (1983) Statistical mechanics of neocortical interactions. Dynamics of synaptic modification. *Phys. Rev. A*, **28**, 395–416.

20 Ingber, L. (2012) Columnar EEG magnetic influences on molecular development of short-term memory, in *Short-Term Memory: New Research* (eds G. Kalivas and S.F. Petralia), Nova, Hauppauge, NY, pp. 37–72.

21 Srinivasan, R., Russell, D.P., Edelman, G. M., and Tononi, G. (1999) Increased synchronization of neuromagnetic responses during conscious perception. *J. Neurosci.*, **19**, 5435–5448.

22 Srinivasan, R. (2004) Internal and external neural synchronization during conscious perception. *Int. J. Bifurcat. Chaos*, **14**, 825–842.

23 Sheinberg, D.L. and Logothetis, N.K. (1997) The role of temporal cortical areas in perceptual organization. *Proc. Natl. Acad. Sci. USA*, **94**, 3408–3413.

24 Logothetis, N.K. (1998) Single units and conscious vision. *Philos. Trans. R. Soc. Lond. B Biol. Sci.*, **353**, 1801–1818.

25 Blake, R. and Logothetis, N.K. (2002) Visual competition. *Nat. Rev. Neurosci.*, **3** (1), 13–21.

26 Gail, A., Brinksmeyer, H.J., and Eckhorn, R. (2004) Perception-related modulations of local field potential power and coherence in primary visual cortex of awake monkey during binocular rivalry. *Cereb. Cortex*, **14** (3), 300–313.

27 Silberstein, R.B. (1995) Steady-state visually evoked potentials, brain resonances, and cognitive processes, in *Neocortical Dynamics and Human EEG Rhythms* (ed. P.L. Nunez), Oxford University Press, pp. 272–303.

28 Brattenberg, V. and Schuz, A. (1991) *Anatomy of the Cortex. Statistics and Geometry*, Springer, New York.

29 Nunez, P.L. (2012) Electric and magnetic fields produced by brain sources, in *Brain–Computer Interfaces for Communication and Control* (eds J.R. Wolpaw and E.W. Wolpaw), Oxford University Press, New York, pp. 45–63.

30 Krieg, W.J.S. (1963) *Connections of the Cerebral Cortex*, Brain Books, Evanston, IL.

31 Krieg, W.J.S. (1973) *Architechtonics of Human Fiber Systems*, Brain Books, Evanston, IL.

32 Koch, C., Rapp, M., and Segev, I. (1996) A brief history of time (constants). *Cereb. Cortex*, **6**, 93–101.

33 Jackson, J.D. (1975) *Classical Electrodynamics*, 2nd edn, John Wiley & Sons, Inc., New York.

34 Nunez, P.L. and Srinivasan, R. (1993) Implications of recording strategy for estimates of neocortical dynamics with EEG. *Chaos*, **3**, 257–266.

35 Jirsa, V.K. and Haken, H. (1997) A derivation of a macroscopic field theory of the brain from the quasi-microscopic neural dynamics. *Physica D*, **99**, 503–526.

36 Sommerhoff, G. (1974) *Logic of the Living Brain*, John Wiley & Sons, Inc., New York.

37 Mountcastle, V.B. (1978) An organizing principle for cerebral function: the unit module and the distributed system, in *The Mindful Brain* (eds G.M. Edelman and V.B. Mountcastle), MIT Press, Cambridge, pp. 7–50.

38 Ingber, L. (1981) Towards a unified brain theory. *J. Soc. Biol. Struct.*, **4**, 211–224.

39 Ingber, L. (1991) Statistical mechanics of neocortical interactions: a scaling paradigm applied to electroencephalography. *Phys. Rev. A*, **44** (6), 4017–4060.

40 Ingber, L. (1994) Statistical mechanics of neocortical interactions: path-integral evolution of short-term memory. *Phys. Rev. E*, **49** (5B), 4652–4664.

41 Ingber, L. (1997) Statistical mechanics of neocortical interactions: applications of canonical momenta indicators to electroencephalography. *Phys. Rev. E*, **55** (4), 4578–4593.

42 Ingber, L. and Nunez, P.L. (1990) Multiple scales of statistical physics of neocortex: application to electroencephalography. *Math. Comput. Model.*, **13** (7), 83–95.

43 Ingber, L. and Nunez, P.L. (1995) Statistical mechanics of neocortical interactions: high resolution path-integral calculation of short-term memory. *Phys. Rev. E*, **51** (5), 5074–5083.

44 Mountcastle, V.B., Andersen, R.A., and Motter, B.C. (1981) The influence of attentive fixation upon the excitability of the light-sensitive neurons of the posterior parietal cortex. *J. Neurosci.*, **1**, 1218–1235.

45 Ingber, L. (1985) Statistical mechanics of neocortical interactions: stability and duration of the 7 ± 2 rule of short-term-memory capacity. *Phys. Rev. A*, **31**, 1183–1186.

46 Ericsson, K.A. and Chase, W.G. (1982) Exceptional memory. *Am. Sci.*, **70**, 607–615.

47 Zhang, G. and Simon, H.A. (1985) STM capacity for Chinese words and idioms: chunking and acoustical loop hypotheses. *Mem. Cognit.*, **13**, 193–201.

48 Hick, W. (1952) On the rate of gains of information. *Q. J. Exp. Psychol.*, **34** (4), 1–33.

49 Ingber, L. (1999) Statistical mechanics of neocortical interactions: reaction time correlates of the *g* factor. *Psycholoquy*, **10**: 1, Invited commentary on the g factor: the science of mental ability by Arthur Jensen, http://www.ingber.com/ smni99_g_factor.pdf.

50 Jensen, A. (1987) Individual differences in the hick paradigm, in *Speed of Information-Processing and Intelligence* (ed. P.A. Vernon) Ablex, Norwood, NJ, pp. 101–175.

51 Ingber, L. (1993) *Adaptive simulated annealing (ASA)*. Technical Report Global optimization C-code, Caltech Alumni Association, Pasadena, CA, http://www. ingber.com/#ASA-CODE.

52 Langouche, F., Roekaerts, D., and Tirapegui, E. (1982) *Functional Integration and Semiclassical Expansions*, Reidel, Dordrecht.

53 Ingber, L. (1985) Statistical mechanics of neocortical interactions. EEG dispersion relations. *IEEE Trans. Biomed. Eng.*, **32**, 91–94.

54 Irimia, A., Swinney, K.R., and Wikswo, J.P. (2009) Partial independence of bioelectric and biomagnetic field and its implications for encephalography and cardiography. *Phys. Rev. E*, **79** (051908), 1–13.

55 Ingber, L. (1998) Statistical mechanics of neocortical interactions: training and testing canonical momenta indicators of EEG. *Math. Comput. Model.*, **27** (3), 33–64.

56 Ingber, L. (2009) Statistical mechanics of neocortical interactions: nonlinear columnar electroencephalography. *NeuroQuantology*, **7** (4), 500–529.

57 Alexander, J.K., Fuss, B., and Colello, R.J. (2006) Electric field-induced astrocyte alignment directs neurite outgrowth. *Neuron Glia Biol.*, **2** (2), 93–103.

58 Georgiev, D. (2003) *Electric and magnetic fields inside neurons and their impact upon the cytoskeletal microtubules.* Technical Report Cogprints Report, Cogprints, University of Southampton, UK, http://cogprints.org/3190/.

59 Murakami, S. and Okada, Y. (2006) Contributions of principal neocortical neurons to magnetoencephalography and electroencephalography signals. *J. Physiol.*, **575** (3), 925–936.

60 Gordon, G.R.J., Iremonger, K.J., Kantevari, S., Ellis-Davies, G.C.R., MacVicar, B.A., and Bains, J.S. (2009) Astrocyte-mediated distributed plasticity at hypothalamic glutamate synapses. *Neuron*, **64**, 391–403.

61 Pereira, A. and Furlan, F.A. (2010) Astrocytes and human cognition: modeling information integration and modulation of neuronal activity. *Prog. Neurobiol.*, **92**, 405–420.

62 Banaclocha, M.A.M. (2007) Neuromagnetic dialogue between neuronal minicolumns and astroglial network: a new approach for memory and cerebral computation. *Brain Res. Bull.*, **73**, 21–27.

63 Ingber, L. (2012) Columnar EEG magnetic influences on molecular development of short-term memory, in *Short-Term Memory: New Research* (eds G. Kalivas and S.F. Petralia), Nova, Hauppauge, NY, pp. 1–36.

64 Ingber, L. (2013) Electroencephalographic field influence on calcium momentum waves, Lester Ingber Research, Ashland, OR. URL http://www.ingber.com/smni13_eeg_ca.pdf